

# Observation of infrared-active modes in Raman scattering from topological insulator nanoplates

Rui He<sup>1</sup>, Zhenhua Wang<sup>2,3</sup>, Richard L J Qiu<sup>2</sup>, Conor Delaney<sup>1</sup>, Ben Beck<sup>1</sup>, T E Kidd<sup>1</sup>, C C Chancey<sup>1</sup> and Xuan P A Gao<sup>2</sup>

<sup>1</sup> Department of Physics, University of Northern Iowa, Cedar Falls, IA 50614-0150, USA

<sup>2</sup> Department of Physics, Case Western Reserve University, Cleveland, OH 44106, USA

<sup>3</sup> Shenyang National Laboratory for Materials Science, Institute of Metal Research, and International Centre for Materials Physics, Chinese Academy of Sciences, 72 Wenhua Road, Shenyang 110016, People's Republic of China


Received 20 July 2012, in final form 5 September 2012

Published 12 October 2012

Online at [stacks.iop.org/Nano/23/455703](http://stacks.iop.org/Nano/23/455703)

## Abstract

Two infrared (IR)-active vibrational modes, observed at 93 and 113 cm<sup>-1</sup> in Raman scattering, are evidence of an inversion symmetry breakdown in thin (~10 nm) nanoplates of topological insulator Bi<sub>2</sub>Te<sub>3</sub> as-grown on SiO<sub>2</sub>. Both Raman and IR modes are preserved after typical device fabrication processes. In nanoplates transferred to another SiO<sub>2</sub> substrate via contact printing, however, the IR modes are absent, and the Raman spectra are similar to those from bulk samples. The differences between as-grown and transferred nanoplates may result from nanoplate–substrate interactions.

 Online supplementary data available from [stacks.iop.org/Nano/23/455703/mmedia](http://stacks.iop.org/Nano/23/455703/mmedia)

(Some figures may appear in colour only in the online journal)

## 1. Introduction

Topological insulators (TIs) represent a new class of quantum system. The interiors of TIs are insulating, but their surfaces and edges are conducting. Interest in three-dimensional (3D) TIs has exploded in recent years following the experimental observation of a single surface state Dirac cone in 3D TI systems such as Bi<sub>2</sub>Se<sub>3</sub>, Bi<sub>2</sub>Te<sub>3</sub>, and Sb<sub>2</sub>Te<sub>3</sub> [1–4]. Characterization of the surface properties of TI materials is crucial to their application in nanoelectronics. 3D TIs in nanostructured forms (e.g. nanoribbons, nanoplates (NPs)) are of particular interest [5–10] since the surface-to-bulk ratio is dramatically increased in low-dimensional systems, which facilitates the observation of surface states. At present, there are a number of extensive studies on the synthesis and electrical transport properties of 3D TI nanostructures [5–7, 10–14], but systematic investigations of phonon properties in TI nanostructures have been more limited [15, 16].

The ability to transfer and manipulate nanomaterials is central to their practical use in electronics [17]. Particularly relevant to the TI research, many experimental investigations

involve mechanical processing and transfers of the sample, which are generally assumed to have no impact on the sample properties. However, if mechanical transfer can change the character of TI nanostructures, then it is important to investigate carefully the sample's fundamental physical properties in different contexts. One case studied here is the comparison between unmanipulated TI NPs on an original substrate ('as-grown') and the characteristics of such as-grown NPs after they have been transferred to a new substrate. Another important issue studied here is the effect of NP thickness on sample characteristics.

In this paper we report the observation of two infrared (IR)-active phonon modes in Raman scattering from as-grown thin (~10 nm) NPs of a representative TI material Bi<sub>2</sub>Te<sub>3</sub>. The two IR modes are centered at 93 and 113 cm<sup>-1</sup> and are tentatively attributed to the out-of-plane vibrations A<sub>1u</sub><sup>1</sup> and A<sub>1u</sub><sup>2</sup>, respectively. This emergence of IR-active modes in Raman spectra reveals a breakdown of inversion symmetry in two-dimensional Bi<sub>2</sub>Te<sub>3</sub>. Both the IR and Raman features remain unchanged after spin-coating with a layer of polymer

and after device fabrication of the NPs, suggesting that the phonon characteristics of the NPs are robust.

Studies of NPs with the same thicknesses but transferred to another SiO<sub>2</sub> substrate show that the IR-active phonon modes are absent and that the Raman spectra are largely similar to those obtained from bulk Bi<sub>2</sub>Te<sub>3</sub>. These results reveal that thickness is not the only parameter that triggers a breakdown of inversion symmetry and a concomitant appearance of IR-active modes in Raman scattering. The absence of inversion symmetry breaking in transferred Bi<sub>2</sub>Te<sub>3</sub> NPs could be ascribed to weak interactions between the NPs and the substrate.

The effect of NP thickness on their vibrational properties is also considered. Evolution of Raman modes as a function of the NP thickness can be interpreted by the phonon dispersion relations, changes in interlayer interactions, disorder-induced inhomogeneous broadening, and changes in electron–phonon interactions in Bi<sub>2</sub>Te<sub>3</sub> NPs.

## 2. Experimental procedures

TI nanostructures have been prepared by various methods, such as chemical vapor deposition [18], molecular beam deposition [9], mechanical exfoliation [8, 13, 16, 19, 20], solvothermal process [21], wet chemical synthesis [15], etc. In this work Bi<sub>2</sub>Te<sub>3</sub> NPs were synthesized on silicon (100) substrate with a 600 nm oxide layer by a vapor-transport-based deposition method at 480 °C in a carrier gas of Ar (10% H<sub>2</sub>), similar to that reported in our previous work on Bi<sub>2</sub>Se<sub>3</sub> nanoribbons [6] and by Kong *et al* [10]. A single-zone tube furnace (Lindberg Blue M) was used for synthesis with accurate control of temperature and gas flow rate. Bi<sub>2</sub>Te<sub>3</sub> powder (99.999%, Alfa Aesar) was ground and placed at the center of the furnace to provide the precursor vapor. The substrates were placed at a distance of 12 cm from the source, downstream of the gas flow. First, a maximum flow rate of 100 standard cubic centimeters per minute (sccm) Ar (10% H<sub>2</sub>) carrier gas was introduced after the system was pumped down to the base pressure of about 8 mTorr. When the temperature of the furnace was increased to 480 °C, the flow rate was decreased to 40 sccm. The pressure was kept at 340 mTorr for 5 min. After that, the furnace was cooled naturally down to room temperature, and dark gray products composed of Bi<sub>2</sub>Te<sub>3</sub> NPs were found on the substrates.

The as-grown NPs were mechanically transferred onto a new silicon wafer (identical to the ones used for growth, with a 600 nm oxide layer) by gently touching the surface of the clean silicon wafer with the NP growth wafer for a few seconds (without sliding). After that, the new Si/SiO<sub>2</sub> wafer was removed from the as-grown substrates, and NPs were found on the new wafer under optical microscopy. This transfer step can be repeated to increase the density of NPs on the new wafer.

Two different surface treatments were conducted to test the robustness of surface properties of the as-grown NPs. The first treatment was to cover the NPs by a polymer layer of poly(methyl methacrylate) (PMMA), a resist used in e-beam-lithography-based device fabrication.

PMMA-950-C2 (about 100 nm thick) was spin-coated at 5000 rpm for 40 s on SiO<sub>2</sub> wafer with as-grown NPs. It was then baked at 180 °C for 8 min. The other surface treatment was to apply standard optical photolithography field effect transistor device fabrication processes on the NPs [22]. This included photoresist (3A and S1805) spin-coating, baking, ultraviolet (UV) light exposure, developing, metal evaporation, and cleaning in a liftoff solvent of PG remover.

Raman scattering is a non-destructive high-resolution spectroscopic probe of the optical, vibrational, and electronic properties of materials. In this study, Raman spectra were taken at room temperature using a Horiba Labram HR Raman Microscope system with 532 nm laser excitation and a thermo-electric cooled charge-coupled device (CCD) detector. A 50× objective lens (numerical aperture of 0.75) was used, and the laser power was kept at about 15 μW in the Raman measurements of thin NPs to avoid laser heating (see supplementary data available at [stacks.iop.org/Nano/23/455703/mmedia](http://stacks.iop.org/Nano/23/455703/mmedia)). This laser excitation power is considered to be safe for the Raman measurements of Bi<sub>2</sub>Te<sub>3</sub> ultrathin layers [8]. The spectral resolution was 0.5 cm<sup>-1</sup> using the 1800 groove/mm grating. Atomic force microscopy (AFM) topographical images were obtained using an Agilent 5500 AFM in non-contact mode with NanoWorld Pointprobe NCHR tips.

## 3. Results and discussions

Figure 1(a) shows an optical image of an as-grown Bi<sub>2</sub>Te<sub>3</sub> NP on a SiO<sub>2</sub> substrate. The NP has a thickness of about 8 nm and shows a weak color contrast with the substrate background. The dark spots are impurities formed during growth. The bright areas show growth of thicker Bi<sub>2</sub>Te<sub>3</sub> layers. AFM images (see figures 1(b) and (c)) show that the NP has a flat surface. A slightly thicker NP of about 11 nm shows a stronger color contrast with the SiO<sub>2</sub> substrate (see figure 1(d)). The surface of this NP is very flat, as shown by the AFM characterization displayed in figures 1(e) and (f). Optical and AFM images of transferred NPs with similar thicknesses are shown in figures 1(g)–(i). Similar to the as-grown NPs, the transferred thin NP of 7 nm shows light green color, and the thicker one of 12 nm is brighter under optical microscopy. The transferred NPs also have reasonably flat surfaces, as shown by AFM scanning.

We present Raman results taken from as-grown and transferred NPs with different thicknesses. Figure 2(a) displays anti-Stokes and Stokes spectra from as-grown thin NPs. A Raman spectrum from bulk Bi<sub>2</sub>Te<sub>3</sub> is included (the top one) for comparison. As-grown thick plates (about 0.5 μm thick) are used as a benchmark for bulk Bi<sub>2</sub>Te<sub>3</sub>. The bulk Bi<sub>2</sub>Te<sub>3</sub> shows four Raman peaks, as highlighted by the dashed vertical lines, which have been assigned to even-parity phonons with A<sub>1g</sub> and E<sub>g</sub> symmetries [23, 24]. Vibrational modes from these four Raman lines are shown in figure 2(b) [23, 24]. The two A<sub>1g</sub> modes are out-of-plane modes from in-phase (lower frequency with superscript 1) and out-of-phase (higher frequency with superscript 2) vibrations of Bi–Te<sup>1</sup> pairs. Similarly, the two E<sub>g</sub>-symmetry modes are

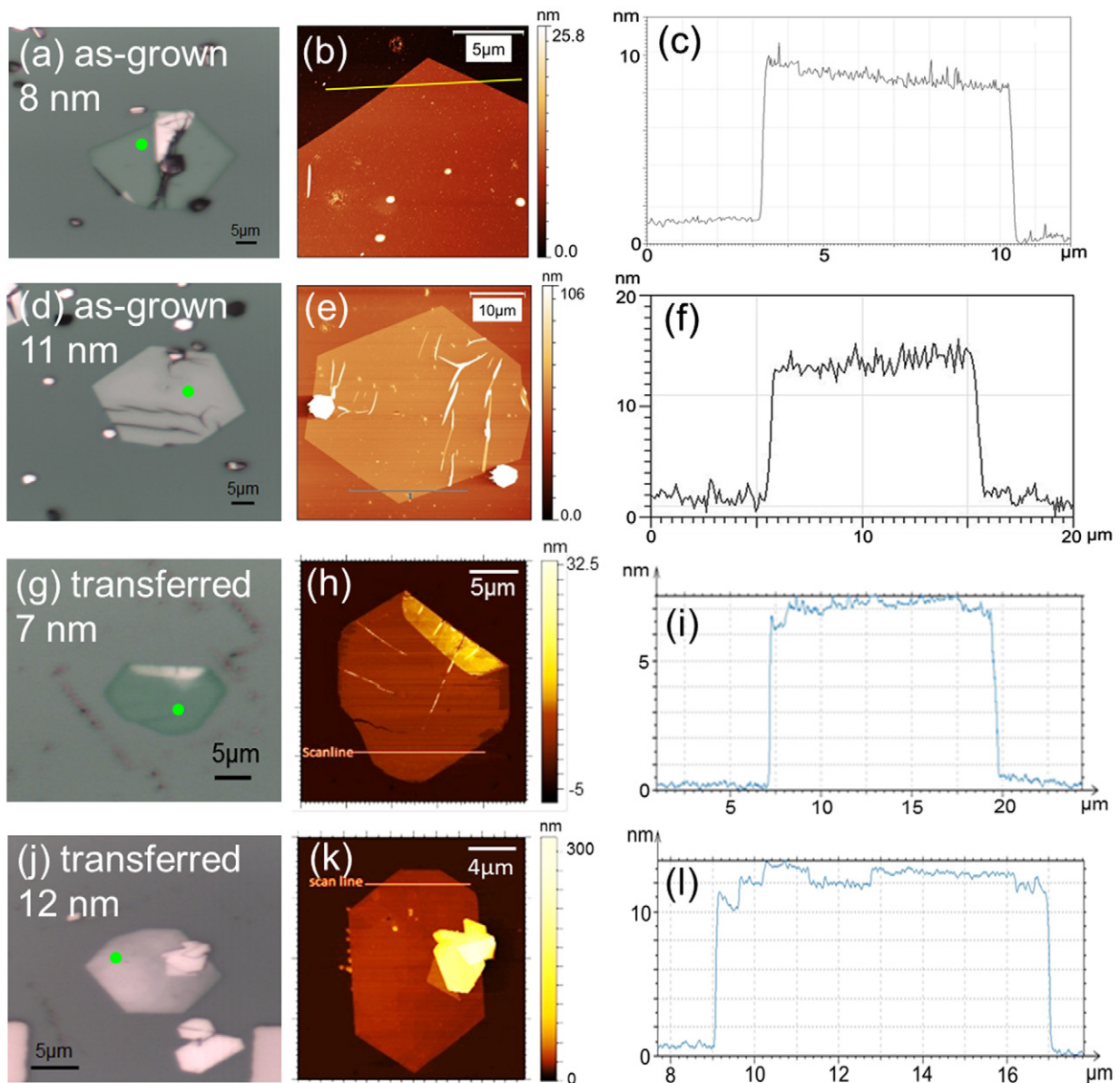


**Figure 1.** (a) Optical image of an as-grown  $\text{Bi}_2\text{Te}_3$  NP on a  $\text{SiO}_2$  substrate. The NP has a thickness of 8 nm and shows a weak color contrast with the substrate background. The irregular spots on the  $\text{SiO}_2$  substrate and the NP are impurity particles from vapor deposition, and the larger bright areas on the NP are thicker  $\text{Bi}_2\text{Te}_3$  layers which do not completely cover the whole area of the NP. The laser focuses on the spot where the bright green dot is. (b) AFM image of the NP shown in panel (a). To improve color contrast, only a corner of the NP is shown. (c) Step height of the NP along the scan line (the solid line) shown in panel (b). (d)–(f), (g)–(i), and (j)–(l) Same as in panels (a)–(c) for an as-grown NP of 11 nm thick, a transferred NP of 7 nm thick, and a transferred NP of 12 nm thick, respectively.

in-phase and out-of-phase modes of in-plane vibrations of  $\text{Bi-Te}^1$  pairs.

In figure 2(a) we see that Raman spectra from as-grown thin NPs differ dramatically from those of the bulk. We focus on the three well-defined Raman modes  $A_{1g}^1$ ,  $E_g^2$ , and  $A_{1g}^2$ . The two out-of-plane modes  $A_{1g}^1$  and  $A_{1g}^2$  shift to lower frequencies in the thin NPs, whereas the in-plane vibrational mode  $E_g^2$  remains unshifted. This observation indicates that the frequencies of the out-of-plane vibrations are more sensitive than in-plane modes to reductions in thickness, and thus are more sensitive to the surface properties of the NPs. Interestingly, two new modes centered at 93 and 113  $\text{cm}^{-1}$

appear in the Raman spectra from the thin NPs (highlighted by solid vertical lines in the lower two spectra in figure 2(a)). Figure 2(c) shows a fit of the spectrum from the 8 nm thick NP with Lorentzian/Fano line shapes [15]. The frequency of the lower energy new mode is very close to that of the lower frequency out-of-plane IR-active vibration ( $A_{1u}^1$  at 94  $\text{cm}^{-1}$ ) and of the higher frequency in-plane IR-active mode ( $E_u^2$  at 95  $\text{cm}^{-1}$ ) [24]. Assuming that out-of-plane vibrations are more sensitive to the change of thickness of the NPs, we have tentatively assigned this new mode at 93  $\text{cm}^{-1}$  in the Raman spectra to the out-of-plane vibration  $A_{1u}^1$  (the left inset of figure 2(c)). The frequency of the other new mode

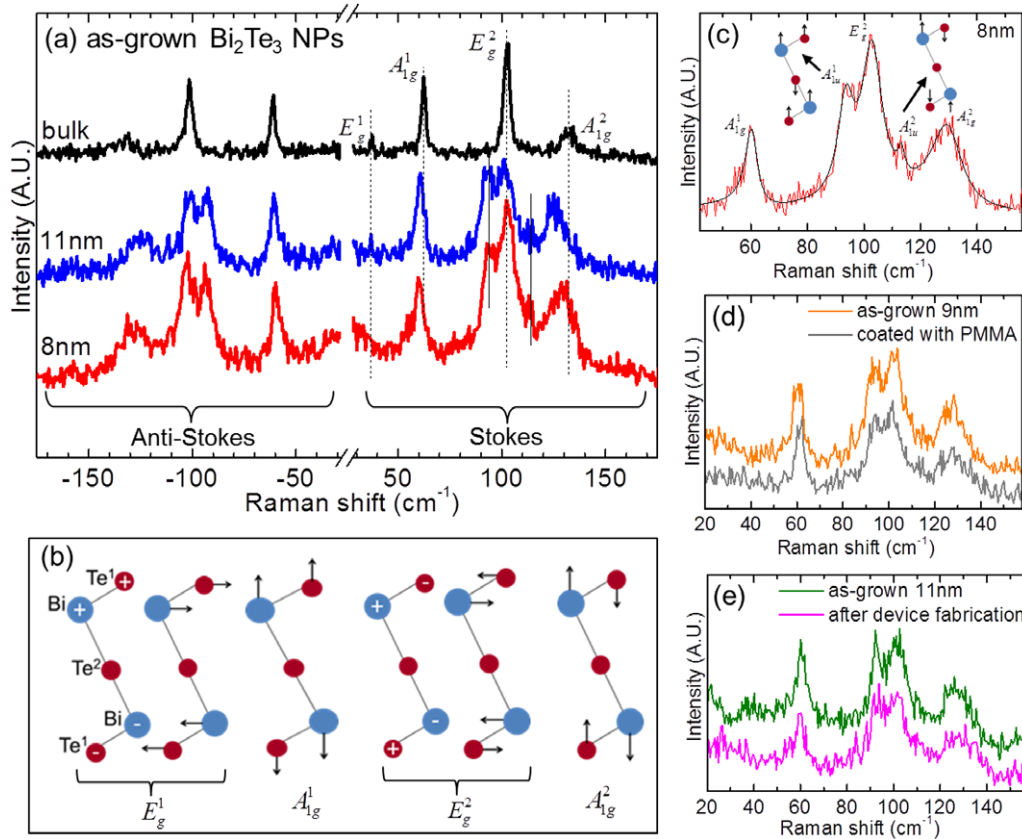


**Figure 2.** (a) Raman spectra from as-grown thin NPs and from bulk Bi<sub>2</sub>Te<sub>3</sub>. Positions of Raman lines from the bulk sample are highlighted by dashed vertical lines, and the positions of IR-active modes in thin NPs are highlighted by solid vertical lines. (b) Raman active modes in Bi<sub>2</sub>Te<sub>3</sub> (for more information see [24]). (c) The black line shows a fit of the Raman peaks with Lorentzian or Fano line shapes. The A<sub>1g</sub><sup>1</sup> and A<sub>1g</sub><sup>2</sup> modes are fit with a Fano line shape. (d) Raman spectra from a NP before and after spin-coating with a PMMA layer of 100 nm thick. (e) Comparison of Raman spectra from a NP before and after device fabrication.

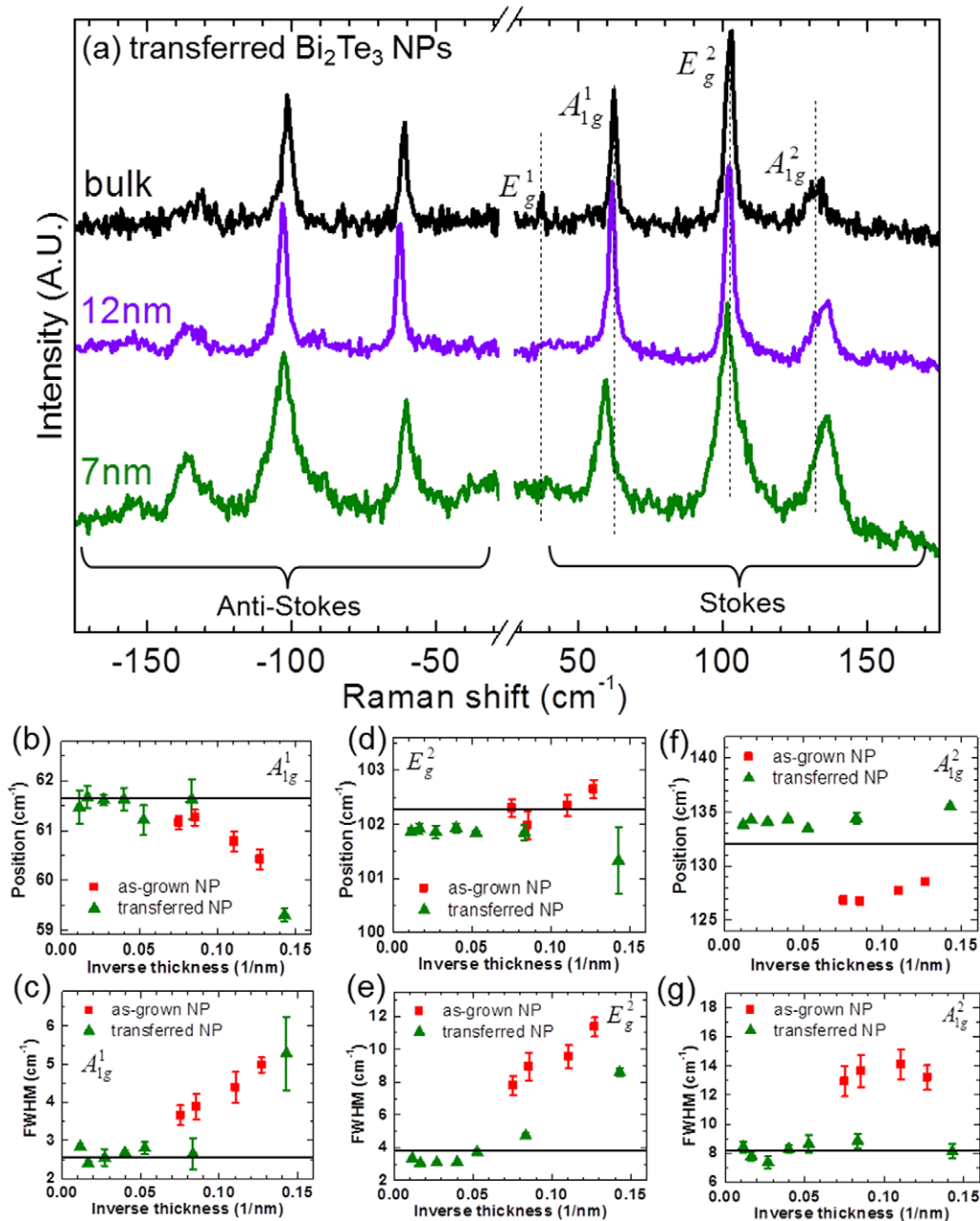
at 113 cm<sup>-1</sup> in the Raman spectra from the as-grown thin NPs is very close to that of the A<sub>1u</sub><sup>2</sup> mode in crystals of Bi<sub>2</sub>Te<sub>3</sub> [24]. Hence, this mode was assigned to the higher frequency out-of-plane IR-active mode A<sub>1u</sub><sup>2</sup> (the right inset of figure 2(c)). In systems with inversion symmetry (such as bulk Bi<sub>2</sub>Te<sub>3</sub>), even-parity phonons are Raman active and odd-parity ones are IR-active. Raman and IR spectroscopies are thus complementary in crystals with a center of inversion. However, in crystals without centers of inversion, phonon modes can be both Raman- and IR-active [25, 26]. The emergence of these two IR-active modes, A<sub>1u</sub><sup>1</sup> at 93 cm<sup>-1</sup> and A<sub>1u</sub><sup>2</sup> at 113 cm<sup>-1</sup>, in Raman spectra thus reveals a breakdown of inversion symmetry in the pristine Bi<sub>2</sub>Te<sub>3</sub> NPs grown by vapor deposition. The presence of the A<sub>1u</sub><sup>2</sup> mode in Raman scattering has been seen in mechanically exfoliated flakes of Bi<sub>2</sub>Te<sub>3</sub> [16] and in hexagonal Bi<sub>2</sub>Te<sub>3</sub> NPs synthesized by a solvothermal process with Bi<sub>2</sub>O<sub>3</sub> as the Bi source [21].

Figure 2(d) shows Raman spectra from an as-grown thin NP before and after spin-coating with a 100 nm thick layer of PMMA. Figure 2(e) displays Raman spectra from an as-grown thin NP before and after a series of device fabrication processes (optical lithography, nickel metal deposition and liftoff). It is seen that the Raman and IR features from the NPs do not change after polymer coating and device

fabrication. These observations suggest that phonon features of the as-grown thin NPs are robust and do not change easily with conventional fabrication processes.

The surfaces of the SiO<sub>2</sub> substrate and of the as-grown Bi<sub>2</sub>Te<sub>3</sub> NPs have many impurities after the vapor-deposition-based growth process (seen as the irregularly shaped spots/particles in the optical images shown in figures 1(a) and (d)). These impurities do not show Raman/IR peaks that overlap those from the NPs (see figure S2 in supplementary data available at [stacks.iop.org/Nano/23/455703/mmedia](http://stacks.iop.org/Nano/23/455703/mmedia)). A simple mechanical transfer process of the NPs to a clean Si/SiO<sub>2</sub> wafer is used to reduce the number of these unwanted particles on the substrate. Figures 1(g)–(l) show optical and AFM images of transferred NPs. We see that these NPs have much cleaner surfaces, whose flatness is largely preserved after transfer, and that the SiO<sub>2</sub> substrate is also free of irregular particles. Figure 3(a) displays Raman spectra from thin transferred NPs and compares them with those from bulk Bi<sub>2</sub>Te<sub>3</sub>. The spectra show that phonon modes from thin transferred NPs are very similar to those from the bulk. The two IR-active modes seen in as-grown thin NPs (figure 2(a)) are absent in the transferred NPs of similar thicknesses. These striking results indicate that the reduction in thickness is not a sufficient condition to induce a breakdown of inversion symmetry in TI nanostructures.





**Figure 3.** (a) Raman spectra from transferred thin NPs and from bulk  $\text{Bi}_2\text{Te}_3$ . Positions of Raman lines from the bulk sample are highlighted by dashed vertical lines. (b)–(g) Positions and FWHM of the  $A_{1g}^1$ ,  $E_g^2$ , and  $A_{1g}^2$  modes from as-grown and transferred NPs as a function of inverse thickness of the NPs. The solid lines show the respective values in bulk  $\text{Bi}_2\text{Te}_3$ .

The reason for the absence of IR-active modes (or inversion symmetry breaking) in transferred NPs could be related to the weak interfacial interaction between the  $\text{SiO}_2$  surface and the NPs. We have observed that there are NPs either lying flat or standing up on their edges on  $\text{SiO}_2$  surfaces (similar to what is seen in samples grown by metalorganic chemical vapor deposition) [27]. The as-grown NPs that we probed by Raman scattering (shown in figure 2(a)) are the ones that lie flat on the substrate. Unlike the ones standing up on edge, these flat-lying as-grown NPs have a strong interaction with the  $\text{SiO}_2$  surface and do not detach easily from it. Supporting evidence is the observation that the

flat-lying as-grown NPs remain intact on the substrate even after ultrasonic cleaning. Therefore, we conjecture that the transfer process only selects those NPs that stand on edge on the substrate after growth. This scenario implies that the  $\text{SiO}_2$  surface forms a relatively strong interaction with the flat-lying thin NPs during growth which induces a breakdown of inversion symmetry in these NPs. This inversion symmetry breaking in as-grown thin NPs could be induced by strain due to a lattice mismatch between  $\text{SiO}_2$  and the  $\text{Bi}_2\text{Te}_3$  NP crystal or perhaps by a charge transfer between the substrate and NPs, which could influence the local electronic properties of the  $\text{Bi}_2\text{Te}_3$  layers at the interface. However,

the transferred NPs may have imperfect contact with the SiO<sub>2</sub> surface and much weaker interaction/bonding with the substrate than the ones directly grown on SiO<sub>2</sub> via a lattice mismatched epitaxial growth process. Substrate-induced inversion symmetry breaking would be absent in these NPs, and thus IR-active modes would not be observed in Raman scattering.

Figures 3(b)–(g) show evolutions of the three well-defined Raman lines  $A_{1g}^1$ ,  $E_g^2$ , and  $A_{1g}^2$  as a function of inverse thickness of the as-grown and transferred NPs. The solid lines in each panel show the respective values in bulk Bi<sub>2</sub>Te<sub>3</sub>. It is seen in figures 3(b) and (c) that features of the  $A_{1g}^1$  phonon from both types of NPs follow the same trend. For NPs thicker than 12 nm, the frequency and full-width-at-half-maximum (FWHM) of the  $A_{1g}^1$  mode are very close to those observed in the bulk. In NPs thinner than 12 nm, this mode displays a redshift and a significant broadening. The redshift could be due to two reasons. The first possibility could be linked to the confinement effect in the nanostructures. The zone center phonon selection rule is relaxed in nanostructured materials [28]. Raman spectra from two-dimensional Bi<sub>2</sub>Te<sub>3</sub> NPs may thus have contributions from phonons away from the Brillouin zone center ( $\Gamma$  point) [15, 28]. The phonon dispersion relation in Bi<sub>2</sub>Te<sub>3</sub> shows that the  $A_{1g}^1$  mode displays a redshift away from the  $\Gamma$  point [29, 30], which would lead to a softening of this phonon in ultrathin NPs. The second possible reason for the softening of this  $A_{1g}^1$  out-of-plane mode could be a reduction of interlayer interactions in the lattice of ultrathin Bi<sub>2</sub>Te<sub>3</sub> NPs [15]. The enhanced broadening of the  $A_{1g}^1$  mode in NPs thinner than 12 nm (figure 3(c)) could be attributed to a disorder-induced inhomogeneous broadening, commonly seen in nanostructures [31–34], or a stronger electron–phonon interaction with a concomitant reduction of phonon lifetime in these ultrathin NPs [15].

Figure 3(d) shows that the position of the in-plane vibrational mode  $E_g^2$  is very close to that from the bulk and does not show a significant change as a function of the thickness of the NPs. This is consistent with the almost flat dispersion of this phonon [29], and it suggests that the frequency of in-plane vibrations is not very sensitive to changes in thickness. In contrast, the FWHM of this  $E_g^2$  mode increases dramatically in NPs thinner than 12 nm (see figure 3(e)). This broadened width could also be linked to inhomogeneous broadening and a stronger electron–phonon interaction in ultrathin NPs. Figure 3(e) also shows that the FWHM of this mode is larger in the as-grown NPs. This enhanced broadening could be linked to a stronger interaction between the NPs and the substrate and a concomitant stronger strain in the as-grown NPs in comparison to the transferred ones.

Figure 3(f) shows the thickness dependence of the position of the  $A_{1g}^2$  phonon. Unlike the  $A_{1g}^1$  mode, which softens in thinner NPs, the position of the  $A_{1g}^2$  mode does not show a clear trend as the thickness of NP decreases. This could be due to two reasons. One reason could be related to the confinement in nanostructures and the resulting dispersion of this phonon mode. The  $A_{1g}^2$  phonon displays

a nonmonotonic dispersion [29]. Phonons away from the Brillouin zone center may have frequencies higher or lower than the zone center frequency. Because of confinement in nanostructures, phonons with nonzero wavevectors whose frequencies could be higher or lower than its zone center value could contribute to the Raman spectra. Hence, the position of the  $A_{1g}^2$  mode does not show a monotonic dependence on the NP thickness. The second reason could be linked to the nature of vibrations of the  $A_{1g}^2$  mode. This out-of-plane mode originates from out-of-phase vibrations of the Bi–Te<sup>1</sup> pairs (see figure 2(b)). We speculate that this vibrational mode may not be as sensitive to the inter-quintuple interactions as the  $A_{1g}^1$  mode is (from in-phase vibrations of Bi–Te<sup>1</sup> pairs). Unlike the monotonic decrease of the position of the  $A_{1g}^1$  mode, the  $A_{1g}^2$  frequency does not show a clear trend as the NP thickness is reduced.

In figures 3(f) and (g) we see that for as-grown NPs the  $A_{1g}^2$  frequency is lower than that from the bulk. Whereas for transferred NPs, the frequency of this mode is higher than that from the bulk. The FWHM of the  $A_{1g}^2$  mode from transferred NPs are similar to that from the bulk. However, the bandwidths of this mode from the as-grown NPs are much broader. The reason for this difference in the positions and FWHM of this  $A_{1g}^2$  mode from the two types of NPs is still unclear. One possible reason for the larger FWHM in the as-grown NPs could be the strain applied by the substrate. This out-of-plane mode is assigned to the out-of-phase vibrations between the Te<sup>1</sup> and Bi atoms (see figure 2(b)). Hence, this mode could be sensitive to the interlayer interactions within a quintuple, which could be different in the as-grown and transferred NPs. This difference in interlayer interaction in the two types of NPs could lead to a change in the  $A_{1g}^2$  phonon frequency.

#### 4. Conclusions

These results show that substrate-induced interactions on Bi<sub>2</sub>Te<sub>3</sub> NPs can have a significant effect on NP characteristics, leading to a breakdown of inversion symmetry. Furthermore, while Bi<sub>2</sub>Te<sub>3</sub> NPs are robust with regards to standard device fabrication techniques, their properties could be impacted by the methods used to transfer NPs to another substrate. Further investigations of less invasive transfer methods, for instance, using PMMA and etching of SiO<sub>2</sub> [35], will further the understanding of NP–substrate interactions.

#### Acknowledgments

RH and TEK acknowledge support from UNI Faculty Summer Fellowships and an Iowa NASA EPSCoR Research Fellowship. ZHW acknowledges the China Scholarship Council for a scholarship supporting her visit to CWRU. XPAG acknowledges the NSF CAREER Award program (grant number DMR-1151534) and the donors of the American Chemical Society Petroleum Research Fund (grant number 48800-DNI10) for financial support of research at CWRU.

## References

- [1] Chen Y L *et al* 2009 Experimental realization of a three-dimensional topological insulator,  $\text{Bi}_2\text{Te}_3$  *Science* **325** 178–81
- [2] Xia Y *et al* 2009 Observation of a large-gap topological-insulator class with a single Dirac cone on the surface *Nature Phys.* **5** 398–402
- [3] Pan Z H, Vescovo E, Fedorov A V, Gardner D, Lee Y S, Chu S, Gu G D and Valla T 2011 Electronic structure of the topological insulator  $\text{Bi}_2\text{Se}_3$  using angle-resolved photoemission spectroscopy: evidence for a nearly full surface spin polarization *Phys. Rev. Lett.* **106** 257004
- [4] Zhang H J, Liu C X, Qi X L, Dai X, Fang Z and Zhang S C 2009 Topological insulators in  $\text{Bi}_2\text{Se}_3$ ,  $\text{Bi}_2\text{Te}_3$  and  $\text{Sb}_2\text{Te}_3$  with a single Dirac cone on the surface *Nature Phys.* **5** 438–42
- [5] Peng H L, Lai K J, Kong D S, Meister S, Chen Y L, Qi X L, Zhang S C, Shen Z X and Cui Y 2010 Aharonov–Bohm interference in topological insulator nanoribbons *Nature Mater.* **9** 225–9
- [6] Tang H, Liang D, Qiu R L J and Gao X P A 2011 Two-dimensional transport-induced linear magneto-resistance in topological insulator  $\text{Bi}_2\text{Se}_3$  nanoribbons *ACS Nano* **5** 7510–6
- [7] Steinberg H, Gardner D R, Lee Y S and Jarillo-Herrero P 2010 Surface state transport and ambipolar electric field effect in  $\text{Bi}_2\text{Se}_3$  nanodevices *Nano Lett.* **10** 5032–6
- [8] Teweldebrhan D, Goyal V and Balandin A A 2010 Exfoliation and characterization of bismuth telluride atomic quintuples and quasi-two-dimensional crystals *Nano Lett.* **10** 1209–18
- [9] Zhang G H, Qin H J, Teng J, Guo J D, Guo Q L, Dai X, Fang Z and Wu K H 2009 Quintuple-layer epitaxy of thin films of topological insulator  $\text{Bi}_2\text{Se}_3$  *Appl. Phys. Lett.* **95** 053114
- [10] Kong D S, Dang W H, Cha J J, Li H, Meister S, Peng H L, Liu Z F and Cui Y 2010 Few-layer nanoplates of  $\text{Bi}_2\text{Se}_3$  and  $\text{Bi}_2\text{Te}_3$  with highly tunable chemical potential *Nano Lett.* **10** 2245–50
- [11] Xiu F X *et al* 2011 Manipulating surface states in topological insulator nanoribbons *Nature Nanotechnol.* **6** 216–21
- [12] Kong D S *et al* 2011 Ambipolar field effect in the ternary topological insulator  $(\text{Bi}_x\text{Sb}_{1-x})_2\text{Te}_3$  by composition tuning *Nature Nanotechnol.* **6** 705–9
- [13] Li Z G *et al* 2012 Experimental evidence on the Altshuler–Aronov–Spivak interference of the topological surface states in the exfoliated  $\text{Bi}_2\text{Te}_3$  nanoflakes *Appl. Phys. Lett.* **100** 083107
- [14] Sulaev A *et al* 2012 Beta- $\text{Ag}_2\text{Te}$ : a topological insulator with strong anisotropy arXiv:1204.3816
- [15] Zhang J, Peng Z P, Soni A, Zhao Y Y, Xiong Y, Peng B, Wang J B, Dresselhaus M S and Xiong Q H 2011 Raman spectroscopy of few-quintuple layer topological insulator  $\text{Bi}_2\text{Se}_3$  nanoplatelets *Nano Lett.* **11** 2407–14
- [16] Shahil K M F, Hossain M Z, Teweldebrhan D and Balandin A A 2010 Crystal symmetry breaking in few-quintuple  $\text{Bi}_2\text{Te}_3$  films: applications in nanometrology of topological insulators *Appl. Phys. Lett.* **96** 153103
- [17] Fan Z Y, Ho J C, Takahashi T, Yerushalmi R, Takei K, Ford A C, Chueh Y L and Javey A 2009 Toward the development of printable nanowire electronics and sensors *Adv. Mater.* **21** 3730–43
- [18] Yan Y, Liao Z M, Yu F, Wu H C, Jing G Y, Yang Z C, Zhao Q and Yu D P 2012 Synthesis and field emission properties of topological insulator  $\text{Bi}_2\text{Se}_3$  nanoflake arrays *Nanotechnology* **23** 305704
- [19] Liao Z M *et al* 2012 Surface plasmon on topological insulator/dielectric interface enhanced ZnO ultraviolet photoluminescence *AIP Adv.* **2** 022105
- [20] Li Z G *et al* 2011 Visualizing topological insulating  $\text{Bi}_2\text{Te}_3$  quintuple layers on  $\text{SiO}_2$ -capped Si substrates and its contrast optimization *J. Nanosci. Nanotechnol.* **11** 7042–6
- [21] Liang Y J, Wang W Z, Zeng B Q, Zhang G L, Song Y Y, Zhang X Y, Huang J, Li J and Li T 2011 The effect of the Bi source on optical properties of  $\text{Bi}_2\text{Te}_3$  nanostructures *Solid State Commun.* **151** 704–7
- [22] Jaeger R C 2002 *Introduction to Microelectronic Fabrication* vol 5, ed G W Neudeck and R F Pierret (Upper Saddle River, NJ: Prentice Hall)
- [23] Kullmann W, Geurts J, Richter W, Lehner N, Rauh H, Steigenberger U, Eichhorn G and Geick R 1984 Effect of hydrostatic and uniaxial pressure on structural properties and Raman active lattice vibrations in  $\text{Bi}_2\text{Te}_3$  *Phys. Status Solidi b* **125** 131–8
- [24] Richter W, Köhler H and Becker C R 1977 A Raman and far-infrared investigation of phonons in the rhombohedral  $\text{V}_2\text{--VI}_3$  compounds  $\text{Bi}_2\text{Te}_3$ ,  $\text{Bi}_2\text{Se}_3$ ,  $\text{Sb}_2\text{Te}_3$  and  $\text{Bi}_2(\text{Te}_{1-x}\text{Se}_x)_3$  ( $0 < x < 1$ ),  $(\text{Bi}_{1-y}\text{Sb}_y)_2\text{Te}_3$  ( $0 < y < 1$ ) *Phys. Status Solidi b* **84** 619–28
- [25] Hayes W and Loudon R 1978 *Scattering of Light by Crystals* (New York: Wiley)
- [26] Yu P Y and Cardona M 2001 *Fundamentals of Semiconductors—Physics and Materials Properties* (New York: Springer)
- [27] Alegria L D and Petta J R 2012 Controlled MOCVD growth of  $\text{Bi}_2\text{Se}_3$  topological insulator nanoribbons arXiv:1206.3091
- [28] Arora A K, Rajalakshmi M, Ravindran T R and Sivasubramanian V 2007 Raman spectroscopy of optical phonon confinement in nanostructured materials *J. Raman Spectrosc.* **38** 604–17
- [29] Kullmann W, Eichhorn G, Rauh H, Geick R, Eckold G and Steigenberger U 1990 Lattice dynamics and phonon dispersion in the narrow gap semiconductor  $\text{Bi}_2\text{Te}_3$  with sandwich structure *Phys. Status Solidi b* **162** 125–40
- [30] Jenkins J O, Rayne J A and Ure R W 1972 Elastic moduli and phonon properties of  $\text{Bi}_2\text{Te}_3$  *Phys. Rev. B* **5** 3171–84
- [31] Song F, Han M, Liu M, Chen B, Wan J and Wang G 2005 Experimental observation of nanojets formed by heating PbO-coated Pb clusters *Phys. Rev. Lett.* **94** 093401
- [32] Spirkoska D, Abstreiter G and Fontcuberta i Morral A 2008 Size and environment dependence of surface phonon modes of gallium arsenide nanowires as measured by Raman spectroscopy *Nanotechnology* **19** 435704
- [33] Hwang Y N, Park S H and Kim D 1999 Size-dependent surface phonon mode of CdSe quantum dots *Phys. Rev. B* **59** 7285–8
- [34] Konstantinovic M J, Bersier S, Wang X, Hayne M, Lievens P, Silverans R E and Moshchalkov V V 2002 Raman scattering in cluster-deposited nanogranular silicon films *Phys. Rev. B* **66** 161311(R)
- [35] Reina A, Son H B, Jiao L Y, Fan B, Dresselhaus M S, Liu Z F and Kong J 2008 Transferring and identification of single- and few-layer graphene on arbitrary substrates *J. Phys. Chem. C* **112** 17741–4